
Switch Spaces: Learning Product Spaces with Sparse Gating

Shuai Zhang¹ Yi Tay² Wenqi Jiang¹ Da-cheng Juan² Ce Zhang¹

Abstract

Learning embedding spaces of suitable geometry is critical for representation learning. In order for learned representations to be effective and efficient, it is ideal that the geometric inductive bias aligns well with the underlying structure of the data. In this paper, we propose Switch Spaces, a data-driven approach for learning representations in product space. Specifically, product spaces (or manifolds) are spaces of mixed curvature, i.e., a combination of multiple euclidean and non-euclidean (hyperbolic, spherical) manifolds. To this end, we introduce sparse gating mechanisms that learn to choose, combine and switch spaces, allowing them to be switchable depending on the input data with specialization. Additionally, the proposed method is also efficient and has a constant computational complexity regardless of the model size. Experiments on knowledge graph completion and item recommendations show that the proposed switch space achieves new state-of-the-art performances, outperforming pure product spaces and recently proposed task-specific models.

1. Introduction

Many machine learning applications involve representation learning (Bengio et al., 2013). Euclidean and recently non-Euclidean spaces have demonstrated successful applications in modeling data with certain structures in various fields. Euclidean space has been extensively studied in the literature and has been serving as the workhorse for decades in representation learning (Bordes et al., 2013; Mikolov et al., 2013; Hsieh et al., 2017). Non-Euclidean space has gained increasing attention as it excels at modeling data with hierarchical or cyclical structures (Wilson et al., 2014; Nickel & Kiela, 2017; Chami et al., 2020b; Vinh Tran et al., 2020; Meng et al., 2019). Until recently, combining multiple

spaces (component spaces) to learn product representations has been proposed and has shown promising results (Gu et al., 2019; Skopek et al., 2020). The main reason for this design is that our data is generated with multiple structures and has varying patterns, rather than be uniformly structured. Models with single type of manifold usually fail in capturing the underlying structures and can cause higher distortion in representation. Product space is an ideal choice as it mixes different types of geometric models as an ensemble which is more suitable for complex and intricate input data.

However, in the existing product-space models, after the spaces are determined (e.g., spherical space \times hyperbolic space), training samples are used to fit the learnable parameters in all these spaces, regardless of the appropriateness (e.g., both spherical and hyperbolic spaces will be updated even if the structure of inputs only aligns with the spherical space). It is difficult to align the geometry of input data with its suitable manifolds via simple combination of spaces without any specialization. Clearly, samples with different geometric structures should be handled with different component spaces. It is essential for component space models to calibrate their internal parameters by focusing on the subset of the training cases that fit the manifold and ignore cases they are not good at modeling. Nevertheless, the intricacy of real-world data makes it impossible to explicitly obtain the exact underlying geometry, let alone partition them into subsets.

To tackle this problem, we propose switch spaces, a data-driven representation approach that automatically chooses suitable spaces for each input data point based on the input-output relationship. Specifically, a sparse gating mechanism is introduced for automatic spaces selection. In this framework, only a certain number of spaces are active in calculation for each incoming sample, which encourages specialization and modularity. Moreover, it enables exploration of various combinations of spaces. Concretely, it can construct a number of smaller product spaces with different signatures based on the given data, allowing to display a greater variety of behaviors. We redefine the scoring function in switch spaces which subsumes the squared distances of product spaces but offers more flexibility. In addition, the computation cost of switch spaces is linear to the number of active spaces, thus making building larger models possible.

¹Department of Computer Science, ETH Zurich, Switzerland
²Google Research, United States. Correspondence to: Shuai Zhang <shuai.zhang@inf.ethz.ch>.

The contributions of this paper are: (a) We propose a representation learning framework, switch spaces, which learn to choose, combine and switch spaces via a sparse gating mechanism. It effectively aligns different types of geometric spaces with the characteristics of the input data, while being computationally efficient; (b) We construct models with switch spaces for two tasks including knowledge graph completion and item recommendation and verify its effectiveness with four real-world datasets. Empirical experiments show that switch spaces constantly outperforms pure product spaces with same signature. With switch spaces, we are able to achieve the state-of-the-art performances on both tasks, outperforming various recent baselines; (c) We conduct model analysis to inspect the inner workings of switch spaces and study the effects of certain modeling choices, to provide insights for extension to other applications.

2. Related Work

In recent years, Non-Euclidean geometric representation learning has gained increasing interests. For example, Hyperbolic representation learning has shown promising performance on a number of tasks such as taxonomic entities modeling (Nickel & Kiela, 2017), network embeddings (Nickel & Kiela, 2017), recommender systems (Vinh Tran et al., 2020), question answering (Tay et al., 2018), knowledge graphs completion (Balazevic et al., 2019a; Chami et al., 2020b), graph-related classification (Chami et al., 2019; Liu et al., 2019), similarity-based hierarchical Clustering (Chami et al., 2020a) and the list goes on. Hyperbolic space is reminiscent of continuous version of trees and excels in modeling hierarchical structures, while spherical space is a more suitable choice for directional similarity modeling and cyclical-structured data. We can find applications of spherical spaces in text embeddings (Meng et al., 2019), texture mapping (Wilson et al., 2014), time-warping functions embedding (Wilson et al., 2014). As indicated, different space has its own specialities and the choice of spaces varies based on the characteristics of data.

To disburden from space selection, product spaces come into play. A product space is a combination of embedding spaces with heterogeneous curvature (e.g., Euclidean space, hyperbolic space, and spherical space, etc.) (Gu et al., 2019; Skopek et al., 2020). Each component of product space has a constant curvature while the resulting mixed space has non-constant curvature, which makes it possible to capture a wider range of curvatures with lower distortion than single space. Theoretically, product space is well-suited for modeling real-world data with mixture structures. Empirically, product spaces demonstrate its efficacy in graph reconstruction, wording embedding with low dimensions (Gu et al., 2019), and image reconstruction (Skopek et al., 2020).

Another line of work that is related this paper is mixture

of experts (MOE) (Jacobs et al., 1991; Jordan & Jacobs, 1994). MOE is established based on the divide-and-conquer principle. It divides problem into homogeneous regions and an expert is responsible for each region. The final prediction is arrived based on the cooperation between experts via a gating network. As a controller, the gating networks control the contribution of each experts via a probabilistic gating function. MOE has been extensively studied in a wide spectrum of applications such as language modeling and machine translation (Shazeer et al., 2017), multi-task learning (Ma et al., 2018), etc. Various MOE architectures have also been proposed in the past decades including hierarchical structure (Yao et al., 2009), sequential experts (Aljundi et al., 2017), deep MOE (Eigen et al., 2013), sparsely-gated MOE (Shazeer et al., 2017), etc.

Different from previous work on product spaces, our work integrate the gating mechanism of MOE (Shazeer et al., 2017) and propose the more expressive switch space, which is a generalization of product space but offers better specialization, higher degree of freedom, and superior computational efficiency.

3. The Geometry of Product Spaces

Stereographic Projection model In general, there are three types of constant curvature spaces with respect to the sign of the curvature. Common realizations are Euclidean space \mathbb{E} (flat), hypersphere \mathbb{S} (positively curved) and hyperboloid \mathbb{H} (negatively curved). For the latter two, we prefer their stereographic projection model: projected sphere \mathbb{D} and Poincare ball \mathbb{P} . These models are easier to optimize, avoiding the problem of non-convergence of norm of points with curvature close to 0, and the projection is conformal, i.e., does not affect the angles between points (Nickel & Kiela, 2017; Skopek et al., 2020).

An alternative to vector space in non-Euclidean geometry is gyrovector space (Ungar, 1991), which defines operations such as vector addition and multiplication. For \mathbb{D} and \mathbb{P} (jointly denoted as \mathcal{M}_c , where c denotes curvature), the addition between two points $\mathbf{x}, \mathbf{y} \in \mathcal{M}_c$, also known as Möbius addition \oplus_c (for both signs of c), is defined as:

$$\mathbf{x} \oplus_c \mathbf{y} = \frac{(1 - 2c\langle \mathbf{x}, \mathbf{y} \rangle - c\|\mathbf{y}\|_2^2)\mathbf{x} + (1 + c\|\mathbf{x}\|_2^2)\mathbf{y}}{1 - 2c\langle \mathbf{x}, \mathbf{y} \rangle + c^2\|\mathbf{x}\|_2^2\|\mathbf{y}\|_2^2}, \quad (1)$$

Where $\langle \cdot, \cdot \rangle$ is Euclidean inner product. The distance between points in the gyrovector space is defined as:

$$d_{\mathcal{M}_c}(\mathbf{x}, \mathbf{y}) = \frac{2}{\sqrt{|c|}} \tan_c^{-1}(\sqrt{|c|}\|\mathbf{x} \oplus_c \mathbf{y}\|_2), \quad (2)$$

where \tan_c stands for \tan if $c > 0$ and \tanh if $c < 0$. In both spaces, we have Euclidean geometry when $c \rightarrow 0$. It is easy to prove that: $d_{\mathcal{M}_c}(\mathbf{x}, \mathbf{y}) \xrightarrow{c \rightarrow 0} 2\|\mathbf{x} - \mathbf{y}\|_2$,

which means the gyrospace distance converges to Euclidean distance when limiting c to zero.

Let $\mathcal{T}_x \mathcal{M}_c$ be the tangent space to the point $\mathbf{x} \in \mathcal{M}_c$. Mapping between (Euclidean) tangent space and hyperbolic/spherical space is performed with exponential map: $\mathcal{T}_x \mathcal{M}_c \rightarrow \mathcal{M}_c$ and logarithmic map: $\mathcal{M}_c \rightarrow \mathcal{T}_x \mathcal{M}_c$, which are defined as:

$$\begin{aligned} \log_x^c(\mathbf{y}) &= \frac{2}{\sqrt{|c|\lambda_x^c}} \tan_c^{-1}(\sqrt{|c|} \|\mathbf{x} \oplus_c \mathbf{y}\|_2) \frac{-\mathbf{x} \oplus_c \mathbf{y}}{\|\mathbf{x} \oplus_c \mathbf{y}\|_2} \\ \exp_x^c(\mathbf{v}) &= \mathbf{x} \oplus_c \left(\tan_c \left(\sqrt{|c|} \frac{\lambda_x^c \|\mathbf{v}\|_2}{2} \right) \frac{\mathbf{v}}{\sqrt{|c|} \|\mathbf{v}\|_2} \right), \end{aligned} \quad (3)$$

where λ_x^c is a conformal factor, defined as $\lambda_x^c = 2/(1 + c\|\mathbf{x}\|_2^2)$, used to transform the metric tensors between (Euclidean) tangent space and non-Euclidean space.

Product Spaces The product space is defined as the Cartesian product of multiple spaces with varying dimensionality and curvature. Let \mathcal{P} denote a product space which is composed by N independent component space $\mathcal{M}^{(1)}, \mathcal{M}^{(2)}, \dots, \mathcal{M}^{(N)}$. The mixed space \mathcal{P} has the following form:

$$\mathcal{P} = \bigtimes_{i=1}^N \mathcal{M}^{(i)} = \mathcal{M}^{(1)} \times \mathcal{M}^{(2)} \times \dots \times \mathcal{M}^{(N)}. \quad (4)$$

The product space \mathcal{P} is also equipped with distance function. The squared distances between points $\mathbf{x}, \mathbf{y} \in \mathcal{P}$ is defined as:

$$d_{\mathcal{P}}^2(\mathbf{x}, \mathbf{y}) = \sum_{i=1}^N d_{\mathcal{M}^{(i)}}^2(\mathbf{x}_{\mathcal{M}^{(i)}}, \mathbf{y}_{\mathcal{M}^{(i)}}), \quad (5)$$

where $\mathbf{x}_{\mathcal{M}^{(i)}}$ and $\mathbf{y}_{\mathcal{M}^{(i)}}$ denote the corresponding vectors on the component space $\mathcal{M}^{(i)}$.

Other operations such as exponential map and logarithmic map are element-wise, which means that we can decompose the points into component spaces and apply operations on each component space and then compose them back (e.g., concatenation) to the product space.

The signature (i.e., parametrization) of product space consists of the types of space, the dimensionality and curvature of each space.

4. Switch Spaces

In this section, we motivate and describe the proposed Switch Spaces: a framework for learning product spaces adaptively based on the incoming data. The guiding design principle for Switch Spaces is to endow the learned product spaces model with specialization in a computationally efficient way.

Problem Setup Suppose we have N spaces of different types and $\mathcal{M}_c^{(i)} \in \{\mathbb{E}, \mathbb{D}, \mathbb{P}\}$. The dimensions of the spaces are b_1, b_2, \dots, b_N . The goal of switch spaces is to select K ($1 \leq K < N$) spaces out from the given N spaces for *each* incoming example and make prediction with the selected K ones, making the signature (i.e., the types of component space) of the learned product space switchable.

Product space model is designed for data with mixed patterns. Yet, it is unclear how to construct a product space model that makes data with certain patterns handled by its suitable space. To calibrate each component space and enhance the alignment between data and its suitable geometries, switch spaces utilize the concept of sparse gating. That is, given a pool of spaces, a sparse gating mechanism is integrated to activate a few spaces for each incoming example, assigning data to its suitable product spaces without manual inspection of the inner structure of input data.

Embedding Layer Let $\mathbf{x}_1 = (\mathbf{u}_1, \dots, \mathbf{u}_N), \mathbf{u}_i \in \mathcal{M}_c^{(i)}$ and $\mathbf{x}_2 = (\mathbf{v}_1, \dots, \mathbf{v}_N), \mathbf{v}_i \in \mathcal{M}_c^{(i)}$ denote two points on the switch space. In real world applications, \mathbf{x}_1 and \mathbf{x}_2 can represent different meanings (e.g., users/items in recommender systems, entities/relations in knowledge graphs) and sometimes more than two vectors are needed. For simplicity, we do not distinguish them in this section. We initialize all the embedding vectors \mathbf{x}_1 and \mathbf{x}_2 in tangent space which is beneficial in two-folds: On the one hand, the embedding layer will be further used for the sparse gating network in Euclidean space. On the other, standard Euclidean optimization techniques can be easily applied thanks to the convenient exponential and logarithmic maps. As such, the overall framework can be optimised in a uniform fashion, avoiding the cumbersome Riemannian optimization (Bonnabel, 2013). Exponential map will be applied to recover the hyperbolic/spherical parameters when necessary.

Selecting Top-K Manifolds The sparse gating network is a differentiable data-driven tool to select the most suitable K spaces for each sample.

We provide two options to construct the gating network which mainly differ in the input and hidden layers. The first option is to construct the input layer by concatenating all the embedding vectors to obtain a one-dimensional vector with length $2 \sum_i^N b_i$:

$$\mathbf{x} = [\mathbf{x}_1, \mathbf{x}_2] = [\mathbf{u}_1, \dots, \mathbf{u}_N, \mathbf{v}_1, \dots, \mathbf{v}_N]. \quad (6)$$

Then linear transformations or 1-D convolutions with linear transformations can be applied over \mathbf{x} to transform it into an N dimensional vector.

Another option is only viable when all embedding vectors have the same dimensionality ($b_1 = \dots b_i = \dots b_N$). We concatenate them into a two-dimensional matrix with shape

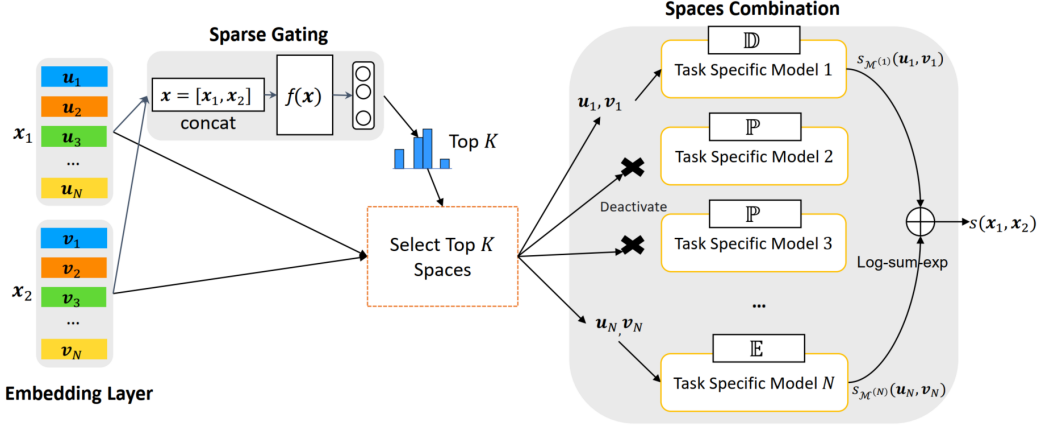


Figure 1. Architecture of the proposed Switch Spaces. Only K out of N spaces are active for each data point.

$2N \times b_i$. Then 2-D convolutions with linear transformations can be applied. Using convolutional operations can in general reduce the number of parameters when b_i is large.

In formal, the last hidden layer of the gating network has the following form:

$$f(\mathbf{x}) = f_1(\mathbf{x}) + \text{randn}() \cdot \ln(1 + \exp(f_2(\mathbf{x}))), \quad (7)$$

where f_1 and f_2 represent linear layers or CNN layers and $f_*(\mathbf{x}) \in \mathbb{R}^N$; function “randn()” creates samples from the standard normal distribution; the second term is a tunable Gaussian noise (only for training) that is added to improve the load balancing, i.e., balance the number of samples accepted by each space.

To impose sparsity, we employ a TopK function to obtain the largest K elements from $f(\mathbf{x})$:

$$f(\mathbf{x}) \leftarrow \text{TopK}(f(\mathbf{x})), \quad (8)$$

where the TopK function returns the original value if the element is in the top K list, otherwise it returns $-\infty$.

We need N gates g_1, g_2, \dots, g_N to generate probabilities to control the activeness of each space.

$$0 \leq g_1(\mathbf{x}), g_2(\mathbf{x}), \dots, g_N(\mathbf{x}) \leq 1, \sum_{i=1}^N g_i(\mathbf{x}) = 1. \quad (9)$$

Simply, a softmax gating network is employed. For $-\infty$, it will output a zero gate value, which introduces sparsity to the gates.

$$g_i(\mathbf{x}) = \frac{\exp(f(\mathbf{x})_i)}{\sum_{j=1}^N \exp(f(\mathbf{x})_j)}. \quad (10)$$

Only spaces with nonzero gate values will be active while other spaces are idle and not computed. In doing so, it provides the possibility to enlarge the model size without incurring much computational cost as long as the number of active spaces K is fixed.

Task Specific Models The model structures are associated with the type of tasks and spaces. In each component space, the input vectors \mathbf{u}_i and \mathbf{v}_i are processed with corresponding exponential/logarithm map for further operations like Mobius addition and distancing function. We elaborate the task specific model in the following section. Let $s_{\mathcal{M}^{(i)}}(\mathbf{u}_i, \mathbf{v}_i)$ (e.g., squared distance, etc.) denote the output of the i^{th} model. We set $s_{\mathcal{M}^{(i)}}$ to 0 if the corresponding space is inactive.

Scoring Function of Switch Space Similar to the definition of squared distance on product space, the scoring function of switch space also decomposes and we defined it as:

$$s(\mathbf{x}_1, \mathbf{x}_2) = \log\left(\sum_{i=1}^N g_i(\mathbf{x}) \exp(s_{\mathcal{M}^{(i)}}(\mathbf{u}_i, \mathbf{v}_i))\right). \quad (11)$$

A log-sum-exp technique is adopted to improve the numerical stability, avoiding problems such as underflow and overflow. Note that multiplying by the gating probability is optional in our framework. If $s_{\mathcal{M}^{(i)}}$ is calculated with squared distance and $K = N$, we can recover the squared distance function defined for product space by removing $g_i(\mathbf{x})$ and the log-sum-exp technique. Our scoring function is not a standard distance metric as it does not satisfy the triangle inequality since we cannot guarantee that two pairs of points have the same active component spaces. In addition, scoring functions other than distance can also be used to allow more complex task-specific models. Relaxing these constraints gives the framework more flexibility.

The architecture of switch space is shown in Figure 1. The whole framework can be optimized end-to-end with model specific loss functions. Also, we add an additional loss function as that discussed in (Shazeer et al., 2017) for load balancing.

Discussion Unlike usual product spaces where the signature is fixed, the signature of the resulting product space in switch spaces may vary according to the gating values. Theoretically, there will be $C_N^K = \frac{N!}{(N-K)!K!}$ possible combinations of product spaces in the switch spaces, allowing greater degree of freedom.

In term of computational complexity, our model has a constant computational cost pertaining to K , regardless of the model sizes (number of model parameters).

In product space, product of $\mathbb{E}^{b_1}, \dots, \mathbb{E}^{b_N}$ is identical to the single space $\mathbb{E}^{b_1+\dots+b_N}$. However, this is not the case in switch space when $K < N$ because the active Euclidean spaces vary.

5. Experiments

In this section, we build models for knowledge graph completions and item recommendations utilizing the proposed switch spaces. Both tasks heavily relies on representation learning. we firstly generalize models into hyperbolic and spherical spaces (if not existed) and then construct the product space and switch space counterparts. We conduct experiments on four real-world datasets and compare with recent proposed baselines. All our experiments are run on NVIDIA TITAN Xp GPUs.

5.1. Knowledge Graph Completion

Knowledge graphs (KG) are fundamental tools for representing information and have applications in wide range of tasks such as question answering and web search. Knowledge graphs are highly incomplete, making it challenging for downstream use. Here, the goal is to infer the missing facts in knowledge graph by embedding the entities and relations into appropriate spaces.

5.1.1. MODEL DETAILS

Given a knowledge graph \mathcal{G} with a set of entities \mathcal{E} and a set of relations \mathcal{R} . Each triplet, abbreviated as (h, r, t) , in \mathcal{G} is composed by two entities (i.e the head entity $h \in \mathcal{E}$ and the tail entity $t \in \mathcal{E}$), and the relationship $r \in \mathcal{R}$ between them.

We follow the base model RotE (Euclidean) and RotH (Poincare) (Chami et al., 2020b) and propose a spherical model. In formal, entities h, t is represented by vectors $\mathbf{e}_h, \mathbf{e}_t \in \mathbb{R}^b$ and relation r is represented by two translation vectors $\alpha_r, \beta_r \in \mathbb{R}^b$ and a rotation vector $\gamma_r \in \mathbb{R}^b$. The head entity is translated twice via Mobius addition in the spherical spaces and rotated once:

$$Q(h, r) = \text{Rot}(\exp_0^c(\mathbf{e}_h) \oplus_c \exp_0^c(\alpha_r), \gamma_r) \oplus_c \exp_0^c(\beta_r), \quad (12)$$

where $c > 0$ and \exp_0^c is the exponential map over origin. Rot is a rotation function and γ_r is the rotation matrix.

| Dataset | $ \mathcal{E} $ | $ \mathcal{R} $ | #training | #val | #test |
|-----------|-----------------|-----------------|-----------|-------|-------|
| WN18RR | 40943 | 11 | 86835 | 3034 | 3134 |
| FB15K-237 | 14541 | 237 | 272115 | 17535 | 20466 |

Table 1. Statistics of the WN18RR and FB15K-237 datasets.

It is then compared with the tail entities using squared spherical distance. The final scoring function is as follows:

$$s(h, r, t) = -d_{\mathcal{M}_c}^2(Q(h, r), \exp_0^c(\mathbf{e}_t)) + b_h + b_t, \quad (13)$$

where $b_h, b_t \in \mathbb{R}$ are head and tail specific biases. Same as RotH, we make the curvature relation specific and trainable. Interested readers are referred to (Chami et al., 2020b) for more details.

We use the above model together with RotE, RotH as the task-specific models for switch space and train the whole framework by minimizing the following cross-entropy loss.

$$\mathcal{L} = \sum_{(h,r,t) \in \Omega} \log(1 + \exp(-Y_{(h,r,t)} s(h, r, t))), \quad (14)$$

where $Y_{(h,r,t)} \in \{1, -1\}$ is a binary label indicating whether a triplet is factual (1) or not (-1). Ω represents the training collection which includes both positive and negative triplets.

For simplicity, we assume that the value of b is identical for all spaces. We concatenate \mathbf{e}_h with α_r and β_r of all spaces and obtain a two dimensional matrix of size $3N \times b$, which is input to the gating network (using 2-D CNN) of switch space. We denote our approach as **SwisE** (short for **Switch Space based KG Embeddings**).

5.1.2. EXPERIMENTAL SETUP

We use two standard datasets including WN18RR (Bordes et al., 2013; Dettmers et al., 2018) and FB15K-237 (Bordes et al., 2013; Dettmers et al., 2018). WN18RR is taken from WordNet, a lexical database of semantic relations between words. FB15K-237 is a subset of the Freebase knowledge graph which is a global resource consisting of common and general information. Statistics of the two datasets is shown in Table 1.

We compare our model with Euclidean methods TransE (Bordes et al., 2013), DistMult (Yang et al., 2015), ConvE (Dettmers et al., 2018), TuckER (Balazevic et al., 2019b), RotE (Chami et al., 2020b), and BoxE (Aboud et al., 2020); complex number based methods ComplEx-N3, (Lacroix et al., 2018) and RotatE (Sun et al., 2019); quaternion model QuatE (Zhang et al., 2019); and hyperbolic methods MurP (Balazevic et al., 2019a) and RotH (Chami et al., 2020b).

The performance of different models are evaluated using two standard metrics including mean reciprocal rank (MRR) and hit rate (HR) with given cut-off value $\{1, 3, 10\}$.

Switch Spaces

| Space | Model | WN18RR | | | | FB15K-237 | | | |
|---------------|--------------|--------------|--------------|--------------|--------------|--------------|--------------|--------------|--------------|
| | | MRR | HR@1 | HR@3 | HR@10 | MRR | HR@1 | HR@3 | HR@10 |
| \mathbb{R} | TransE | 0.226 | - | - | 0.501 | 0.294 | - | - | 0.465 |
| | BoxE | 0.451 | - | - | 0.541 | 0.337 | - | - | 0.538 |
| | DistMult | 0.430 | 0.390 | 0.440 | 0.490 | 0.241 | 0.155 | 0.263 | 0.419 |
| | ConvE | 0.430 | 0.400 | 0.440 | 0.520 | 0.325 | 0.237 | 0.356 | 0.501 |
| | TuckER | 0.470 | 0.443 | 0.482 | 0.526 | 0.358 | 0.266 | 0.394 | 0.544 |
| | RotE | 0.494 | 0.446 | 0.512 | 0.585 | 0.346 | 0.251 | 0.381 | 0.538 |
| \mathbb{C} | ComplEx-N3 | 0.480 | 0.435 | 0.495 | 0.572 | 0.357 | 0.264 | 0.392 | 0.547 |
| | RotatE | 0.476 | 0.428 | 0.492 | 0.571 | 0.338 | 0.241 | 0.375 | 0.533 |
| \mathbb{Q} | QuatE | 0.488 | 0.438 | 0.508 | 0.582 | <u>0.366</u> | <u>0.271</u> | <u>0.401</u> | <u>0.556</u> |
| \mathbb{P} | MurP | 0.481 | 0.440 | 0.495 | 0.566 | 0.335 | 0.243 | 0.367 | 0.518 |
| | RotH | <u>0.496</u> | <u>0.449</u> | <u>0.514</u> | <u>0.586</u> | 0.344 | 0.246 | 0.380 | 0.535 |
| Switch Spaces | SwisE | 0.526 | 0.480 | 0.549 | 0.610 | 0.521 | 0.486 | 0.530 | 0.585 |

Table 2. Comparison with state-of-the-arts on datasets WN18RR and FB15K-237. The best performances are in boldface and the second best are underlined. The performance of switch space on WN18RR is achieved with model $(\mathbb{D}^{100})^4\mathbb{E}^{100}(K=2)$, and that on FB15K-237 is with $(\mathbb{P}^{100})^3(\mathbb{D}^{100})^2(K=4)$. \mathbb{R} :real coordinate space; \mathbb{C} :complex number space; \mathbb{Q} :quaternion space.

| Space | Model | MRR | HR@3 |
|-----------------|--|-------|-------|
| Single | \mathbb{D}^{500} | 0.492 | 0.514 |
| Product | $(\mathbb{P}^{100})^5$ | 0.483 | 0.498 |
| | $(\mathbb{D}^{100})^5$ | 0.480 | 0.506 |
| | $(\mathbb{P}^{100})^3(\mathbb{D}^{100})^2$ | 0.484 | 0.498 |
| | $(\mathbb{D}^{100})^4\mathbb{E}^{100}$ | 0.479 | 0.497 |
| | $(\mathbb{P}^{100})^4\mathbb{E}^{100}$ | 0.477 | 0.498 |
| | $(\mathbb{P}^{100})^2(\mathbb{D}^{100})^2\mathbb{E}^{100}$ | 0.479 | 0.496 |
| Switch (K=2) | $(\mathbb{P}^{100})^5$ | 0.516 | 0.539 |
| | $(\mathbb{D}^{100})^5$ | 0.509 | 0.531 |
| | $(\mathbb{P}^{100})^3(\mathbb{D}^{100})^2$ | 0.500 | 0.521 |
| | $(\mathbb{D}^{100})^4\mathbb{E}^{100}$ | 0.526 | 0.549 |
| | $(\mathbb{P}^{100})^4\mathbb{E}^{100}$ | 0.517 | 0.542 |
| | $(\mathbb{P}^{100})^2(\mathbb{D}^{100})^2\mathbb{E}^{100}$ | 0.522 | 0.546 |

Table 3. Comparison with Product Spaces Models (Only representative signatures are reported due to length constraints).

The total dimension is fixed to 500 for fair comparison. Learning rate is tuned among $\{0.01, 0.005, 0.001\}$. For all experiments, we reports the average over 5 runs. We set the kernel size to 5 and stride to 3 for convolution operation in the gating network. N is set to 5 and K is tuned among $\{1, 2, 3, 4\}$. The number of negative samples size per factual triplet is set to 50. Optimizer Adam is used for model learning.

5.1.3. RESULTS

Comparison with the State-of-the-art Table 2 compares our best scores with baselines. Notably, SwisE achieves the new state-of-the-art results across all metrics on both datasets. SwisE outperforms Euclidean, hyperbolic, complex-valued approaches, and obtains a clear performance gain over the second best baseline. Specif-

ically, the improvement on FB15K-237 is quite impressive, this is because that FB15K-237 has a more diverse set of relations than WN18RR (Balazevic et al., 2019a), which is also the reason why RotH is surpassed by several Euclidean/complex-valued baselines. Additionally, we observe that RotH and QuatE achieve the second best on WN18RR and FB15K-237, respectively.

Comparison with Product Space We compare the switch spaces with product spaces with varying signatures in Table 3 on WN18RR. We observe that switch spaces constantly outperform pure product spaces with the same prior signatures, which ascertains the effectiveness of switch spaces. It is worth noting that SwisE requires merely two active spaces for each instance to outperforms product spaces with five spaces. We find that SwisE with the product of spherical and Euclidean spaces archives better performances than other configurations.

5.2. Item Recommendation

Recommender system is an important part in modern e-commerce platforms. It can improve customers experience via reducing information overload, and increase revenue for companies. Learning representations that reflect users’ preference and items characteristics has been a central theme in item recommendations research (Ricci et al., 2011).

5.2.1. MODEL DETAILS

Given a collection of C_1 users and C_2 items and interactions observed between them, the goal is to produce personalized items recommendation for each user. We are interested in metric learning based collaborative filtering (Hsieh et al., 2017; Vinh Tran et al., 2020). Taken a user vector $\mathbf{u}_u, \mathbf{u} \in$

Switch Spaces

| Space | Model | MovieLens 100K | | | MovieLens 1M | | |
|-----------------|---|------------------|------------------|------------------|------------------|------------------|------------------|
| | | MAP | P@10 | R@10 | Map | P@10 | R@10 |
| Single | BPRMF | .211±.003 | .254±.001 | .176±.004 | .120±.001 | .185±.001 | .078±.001 |
| | \mathbb{E}^{100} (CML) | .195±.001 | .233±.003 | .165±.003 | .138±.002 | .208±.002 | .092±.003 |
| | \mathbb{P}^{100} (HyperML) | .157±.001 | .194±.003 | .136±.004 | .113±.001 | .167±.002 | .075±.002 |
| | \mathbb{D}^{100} | .161±.001 | .193±.002 | .137±.001 | .116±.001 | .170±.004 | .077±.001 |
| Product | $(\mathbb{E}^{20})^5$ | .199±.002 | .240±.001 | .168±.003 | .150±.001 | .221±.002 | .100±.001 |
| | $(\mathbb{P}^{20})^5$ | .169±.003 | .210±.004 | .146±.003 | .128±.003 | .189±.002 | .083±.001 |
| | $(\mathbb{D}^{20})^5$ | .177±.003 | .212±.002 | .149±.005 | .131±.001 | .188±.001 | .085±.004 |
| | $(\mathbb{D}^{20})^3(\mathbb{P}^{20})^2$ | .173±.001 | .209±.001 | .151±.001 | .133±.001 | .193±.001 | .085±.001 |
| | $(\mathbb{P}^{20})^2(\mathbb{D}^{20})^2\mathbb{E}^{20}$ | .176±.001 | .208±.002 | .149±.003 | .134±.002 | .192±.003 | .088±.002 |
| Switch (K=4) | $(\mathbb{E}^{20})^5$ | .218±.003 | .267±.003 | .188±.002 | .158±.001 | .236±.001 | .105±.002 |
| | $(\mathbb{P}^{20})^5$ | .191±.002 | .233±.005 | .162±.004 | .142±.003 | .213±.005 | .094±.005 |
| | $(\mathbb{D}^{20})^5$ | .194±.002 | .233±.005 | .162±.002 | .172±.003 | .253±.003 | .116±.002 |
| | $(\mathbb{D}^{20})^3(\mathbb{P}^{20})^2$ | .203±.003 | .246±.002 | .174±.003 | .174±.001 | .252±.002 | .116±.001 |
| | $(\mathbb{P}^{20})^2(\mathbb{D}^{20})^2\mathbb{E}^{20}$ | .201±.002 | .245±.004 | .171±.001 | .172±.001 | .249±.002 | .114±.002 |

Table 4. Recommendation performances on two benchmark datasets. Only representative signatures are reported due to length constraints.

| Dataset | C_1 | C_2 | #Interactions | density |
|----------------|-------|-------|---------------|---------|
| MovieLens 100K | 943 | 1682 | 100,000 | 0.063 |
| MovieLens 1M | 6040 | 3706 | 1,000,209 | 0.045 |

Table 5. Statistics of MovieLens 100K and MovieLens 1M.

$\mathcal{M}_c^{C_1 \times b}$ and an item vector $\mathbf{v}_i, \mathbf{v} \in \mathcal{M}_c^{C_2 \times b}$ as input. The preference of user u towards item i is measured by the squared distance between them:

$$s(u, i) = -d_{\mathcal{M}_c}^2(\mathbf{u}_u, \mathbf{v}_i). \quad (15)$$

We optimize the model with a max-margin hinge loss.

$$\mathcal{L} = \sum_{(u, i, j) \in \Omega} \max(0, s(u, i) + m - s(u, j)), \quad (16)$$

where Ω is the collection of training samples; i is the item that u liked and j represents a negative (unobserved) item for the user. $\max(0, x)$ is also known as the *ReLU* function. m is a margin value.

We also use the same b for all component spaces for brevity. The input of the gating network is the concatenation of the user and item embeddings. Specifically, a one dimensional vector of size \mathbb{R}^{2Nb} is used as the input and a linear layer is applied in the gating network.

5.2.2. EXPERIMENTAL SETUP

We conduct our experiments on two datasets: MovieLens 100K and MovieLens 1M (Harper & Konstan, 2015). We hold 70% actions in each user’s interactions as the training set, 10% actions as the validation set for model tuning and the remaining 20% actions as the test set. All interactions (e.g., ratings) are binarized following the implicit feedback

setting (Rendle et al., 2009). We estimate the global average curvature with the algorithm described in (Gu et al., 2019) for the two datasets and obtain 0.190 for MovieLens 100K and 0.695 for MovieLens 1M, which suggests that they lean towards Euclidean/cyclical structures. Statistics of them are in Table 5.

We compare our method with a number of baselines including Bayesian personalized ranking based matrix factorization (BPRMF) (Rendle et al., 2009), Euclidean, hyperbolic, spherical, and product space models. \mathbb{E}^n corresponds to CML (Hsieh et al., 2017), \mathbb{P}^n is equivalent to HyperML (Vinh Tran et al., 2020).

We measure the performance based on the widely adopted metrics in recommender systems: mean average precision (MAP), precision ($P@5$ and $P@10$), and recall ($R@5$ and $R@10$).

For all models, the total dimension is fixed to 100 for fair comparison. The curvatures for spherical and hyperbolic models are set to 1 and -1 , respectively. N is set to 5 and K is tuned among $\{1, 2, 3, 4\}$. Regularization rate is chosen from $\{0.1, 0.01, 0.001\}$. m is fixed to 0.5. Adam is also adopted as the optimizer.

5.2.3. RESULTS

Table 4 summarizes the performances of our model. The merits of switch spaces can be further observed from the comparison. On both datasets, switch spaces based models achieve the best performances, outperforming their pure product space counterparts with the same signature. Another clear pattern is that product spaces usually performs better than single spaces. Specifically, on MovieLens 100K, Euclidean space is the most effective. While, on MovieLens

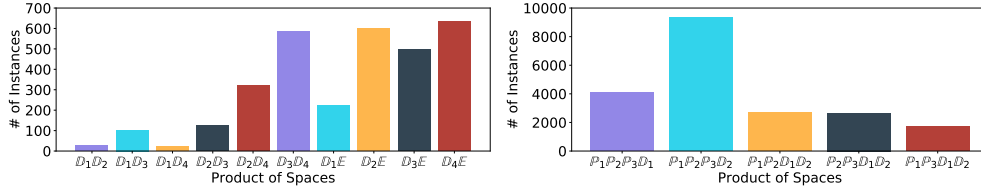


Figure 2. Distribution of the learned spaces on test data of WN18RR (left figure, $(\mathbb{D}^{100})^4 \mathbb{E}^{100}$ ($K = 2$)) and FB15K-237 (right figure, $(\mathbb{P}^{100})^3 (\mathbb{D}^{100})^2$ ($K = 4$)) using switch space.

1M, spherical space dominated models outperform other space related models. This observation is consistent with the global average curvature we estimated. Interestingly, we find that the matrix factorization approach (BPRMF) remains competitive on the two datasets and usually achieves better results than other single space models.

6. Model Analysis

6.1. Distribution of the Learned Spaces

Figure 2 presents the distribution of the learned spaces combinations. It is obvious that samples are not randomly distributed. Instead, certain products are preferred in each case. For example, the product between spherical and Euclidean spaces are more popular on WN18RR. While on FB15K-237, hyperbolic space dominated spaces are preferable. To show more fine-grained examples, we randomly select three relations from FB15K-237. The distribution of samples that contain these relations are shown in Figure 3. We find that relations have their own desirable product spaces as well. This reconfirms the specification capability of the proposed switch spaces.

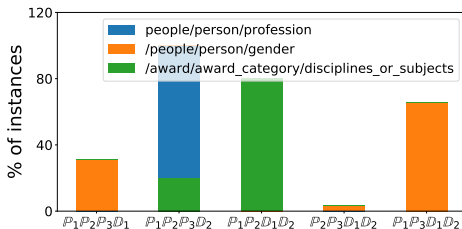


Figure 3. Distribution of the learned spaces of three examples from FB15K-237. Counts of instances are normalized.

6.2. Effects of Total Spaces Number

Figure 4 reports the test MRR and inference time varied across the different N values with $K = 2$ on dataset WN18RR using switch space model $(\mathbb{P}^{100})^N$. We observe that, in this task, the model performance does not benefit from the increasing model size. Also, the inference time remains nearly constant when we increase N , confirming the efficiency of switch spaces. This property is important for tasks (e.g., language modeling) that prefer larger model size.

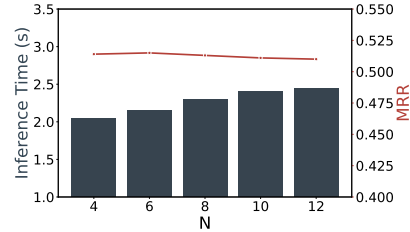


Figure 4. Effect of N with model $(\mathbb{P}^{100})^N$ ($K=2$) on MRR and inference time, on dataset WN18RR.

6.3. Effects of Active Spaces Number

We show the effects of the number of active spaces K in Figure 5. We observe that, compared with N , K has a relatively higher impact on the model performance and inference time cost. On WN18RR, a small K (e.g., 1, 2) value can lead to the optimal performance.

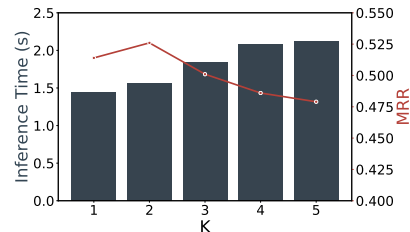


Figure 5. Effect of K with model $(\mathbb{D}^{100})^4 \mathbb{E}^{100}$ on dataset WN18RR.

7. Conclusion

We proposed switch space, a framework for learning expressive product spaces. Switch spaces make use of a sparse gating mechanism to ensure incoming data to be handled by suitable spaces, allowing greater extend of specification in representation. We apply switch space to real world tasks (i.e., knowledge graph completion and item recommendation) and it obtains state-of-the-art performances on benchmark datasets, while being efficient. We believe that switch spaces hold promise for more expressive and generalizable representation learning.

References

Abboud, R., Ceylan, I., Lukasiewicz, T., and Salvatori, T. Boxe: A box embedding model for knowledge base com-

- pletion. *Advances in Neural Information Processing Systems*, 33, 2020.
- Aljundi, R., Chakravarty, P., and Tuytelaars, T. Expert gate: Lifelong learning with a network of experts. In *Proceedings of the IEEE Conference on Computer Vision and Pattern Recognition*, pp. 3366–3375, 2017.
- Balazevic, I., Allen, C., and Hospedales, T. Multi-relational poincaré graph embeddings. In *Advances in Neural Information Processing Systems*, pp. 4463–4473, 2019a.
- Balazevic, I., Allen, C., and Hospedales, T. Tucker: Tensor factorization for knowledge graph completion. In *Proceedings of the 2019 Conference on Empirical Methods in Natural Language Processing and the 9th International Joint Conference on Natural Language Processing (EMNLP-IJCNLP)*, pp. 5188–5197, 2019b.
- Bengio, Y., Courville, A., and Vincent, P. Representation learning: A review and new perspectives. *IEEE transactions on pattern analysis and machine intelligence*, pp. 1798–1828, 2013.
- Bonnabel, S. Stochastic gradient descent on riemannian manifolds. *IEEE Transactions on Automatic Control*, 58(9):2217–2229, 2013.
- Bordes, A., Usunier, N., Garcia-Duran, A., Weston, J., and Yakhnenko, O. Translating embeddings for modeling multi-relational data. *Advances in neural information processing systems*, 26:2787–2795, 2013.
- Chami, I., Ying, Z., Ré, C., and Leskovec, J. Hyperbolic graph convolutional neural networks. In *Advances in neural information processing systems*, pp. 4868–4879, 2019.
- Chami, I., Gu, A., Chatziafratis, V., and Ré, C. From trees to continuous embeddings and back: Hyperbolic hierarchical clustering. *Advances in Neural Information Processing Systems*, 2020a.
- Chami, I., Wolf, A., Juan, D.-C., Sala, F., Ravi, S., and Ré, C. Low-dimensional hyperbolic knowledge graph embeddings. In *Proceedings of the 58th Annual Meeting of the Association for Computational Linguistics*, pp. 6901–6914, Online, July 2020b. Association for Computational Linguistics. doi: 10.18653/v1/2020.acl-main.617. URL <https://www.aclweb.org/anthology/2020.acl-main.617>.
- Dettmers, T., Minervini, P., Stenetorp, P., and Riedel, S. Convolutional 2d knowledge graph embeddings. In *Proceedings of the AAAI Conference on Artificial Intelligence*, volume 32, 2018.
- Eigen, D., Ranzato, M., and Sutskever, I. Learning factored representations in a deep mixture of experts. *arXiv preprint arXiv:1312.4314*, 2013.
- Gu, A., Sala, F., Gunel, B., and Ré, C. Learning mixed-curvature representations in product spaces. In *International Conference on Learning Representations*, 2019.
- Harper, F. M. and Konstan, J. A. The movielens datasets: History and context. *Acm transactions on interactive intelligent systems (tiis)*, 5(4):1–19, 2015.
- Hsieh, C.-K., Yang, L., Cui, Y., Lin, T.-Y., Belongie, S., and Estrin, D. Collaborative metric learning. In *Proceedings of the 26th international conference on world wide web*, pp. 193–201, 2017.
- Jacobs, R. A., Jordan, M. I., Nowlan, S. J., and Hinton, G. E. Adaptive mixtures of local experts. *Neural computation*, 3(1):79–87, 1991.
- Jordan, M. I. and Jacobs, R. A. Hierarchical mixtures of experts and the em algorithm. *Neural computation*, 6(2):181–214, 1994.
- Lacroix, T., Usunier, N., and Obozinski, G. Canonical tensor decomposition for knowledge base completion. In *International Conference on Machine Learning*, pp. 2863–2872, 2018.
- Liu, Q., Nickel, M., and Kiela, D. Hyperbolic graph neural networks. In *Advances in Neural Information Processing Systems*, pp. 8230–8241, 2019.
- Ma, J., Zhao, Z., Yi, X., Chen, J., Hong, L., and Chi, E. H. Modeling task relationships in multi-task learning with multi-gate mixture-of-experts. In *Proceedings of the 24th ACM SIGKDD International Conference on Knowledge Discovery & Data Mining*, pp. 1930–1939, 2018.
- Meng, Y., Huang, J., Wang, G., Zhang, C., Zhuang, H., Kaplan, L., and Han, J. Spherical text embedding. In *Advances in Neural Information Processing Systems*, pp. 8208–8217, 2019.
- Mikolov, T., Chen, K., Corrado, G., and Dean, J. Efficient estimation of word representations in vector space. *arXiv preprint arXiv:1301.3781*, 2013.
- Nickel, M. and Kiela, D. Poincaré embeddings for learning hierarchical representations. In *Advances in neural information processing systems*, pp. 6338–6347, 2017.
- Rendle, S., Freudenthaler, C., Gantner, Z., and Schmidt-Thieme, L. Bpr: Bayesian personalized ranking from implicit feedback. In *Proceedings of the Twenty-Fifth Conference on Uncertainty in Artificial Intelligence*, pp. 452–461, 2009.

- Ricci, F., Rokach, L., and Shapira, B. Introduction to recommender systems handbook. In *Recommender systems handbook*, pp. 1–35. Springer, 2011.
- Shazeer, N., Mirhoseini, A., Maziarz, K., Davis, A., Le, Q., Hinton, G., and Dean, J. Outrageously large neural networks: The sparsely-gated mixture-of-experts layer. *arXiv preprint arXiv:1701.06538*, 2017.
- Skopek, O., Ganea, O.-E., and Bécigneul, G. Mixed-curvature variational autoencoders. In *International Conference on Learning Representations*, 2020.
- Sun, Z., Deng, Z.-H., Nie, J.-Y., and Tang, J. Rotate: Knowledge graph embedding by relational rotation in complex space. In *International Conference on Learning Representations*, 2019.
- Tay, Y., Tuan, L. A., and Hui, S. C. Hyperbolic representation learning for fast and efficient neural question answering. In *Proceedings of the Eleventh ACM International Conference on Web Search and Data Mining*, pp. 583–591, 2018.
- Ungar, A. A. Thomas precession and its associated group-like structure. *American Journal of Physics*, 59(9):824–834, 1991.
- Vinh Tran, L., Tay, Y., Zhang, S., Cong, G., and Li, X. Hyperml: A boosting metric learning approach in hyperbolic space for recommender systems. In *Proceedings of the 13th International Conference on Web Search and Data Mining*, pp. 609–617, 2020.
- Wilson, R. C., Hancock, E. R., Pekalska, E., and Duin, R. P. Spherical and hyperbolic embeddings of data. *IEEE transactions on pattern analysis and machine intelligence*, 36(11):2255–2269, 2014.
- Yang, B., Yih, W.-t., He, X., Gao, J., and Deng, L. Embedding entities and relations for learning and inference in knowledge bases. *ICLR*, 2015.
- Yao, B., Walther, D., Beck, D., and Fei-Fei, L. Hierarchical mixture of classification experts uncovers interactions between brain regions. *Advances in Neural Information Processing Systems*, 22:2178–2186, 2009.
- Zhang, S., Tay, Y., Yao, L., and Liu, Q. Quaternion knowledge graph embeddings. In *Advances in Neural Information Processing Systems*, pp. 2735–2745, 2019.